

Calibrating the Spatial Response of Bio-Optical Sensors

FABIAN WOLK

Rockland Oceanographic Services Inc., Victoria, British Columbia, Canada

HIDEKATSU YAMAZAKI

Department of Ocean Sciences, Tokyo University of Marine Science and Technology, Tokyo, Japan

HUA LI

Alec Electronics Co. Ltd., Kobe, Japan

ROLF G. LUECK

School of Earth and Ocean Science, University of Victoria, Victoria, British Columbia, Canada

(Manuscript received 27 December 2004, in final form 12 July 2005)

ABSTRACT

This article describes an experimental method used to establish the spatial wavenumber response of in situ fluorometers. The method is applied to a fluorometer developed to measure the structure of the fluorescence field at high spatial wavenumbers. This fluorometer detects fluorescence variations on centimeter scales by creating a sampling volume in the undisturbed flow region, outside of the sensor housing. The sampling volume is created by intersecting beams of blue excitation light. To establish the size of the sampling volume and the amount of spatial averaging, the fluorometer and a fast response thermistor are towed repeatedly through a warm, fluorescent plume in a tow tank. The ratio of the measured fluorescence and temperature spectrum determines the wavenumber response of the fluorometer. The measured spectral ratio is well described by the transfer function of a first-order, low-pass filter with a half-power point at 22 cpm. The equivalent spatial resolution is 7 mm. The transfer function model can be used to correct measured fluorescence spectra for the limited wavenumber response of the sensor.

1. Introduction

The distribution and structure of in situ phytoplankton assemblages have been studied for some time (Derenbach et al. 1979; Mann and Lazier 1996), and their structure at submeter scales is of growing interest to marine biologists and physicists. Recent studies on this topic are summarized by Seuront and Strutton (2004).

The power spectrum of scalar tracers, for example, temperature, matches the $-5/3$ slope of the velocity spectrum in the inertial subrange (Batchelor 1967). In the viscous convective subrange, the velocity spectrum has a -1 slope; in this wavenumber region the spectrum

of a scalar tracer departs from the $-5/3$ slope of velocity (Corrsin 1951). Fluorescence, as a tracer of phytoplankton, has traditionally been considered a passive scalar. However, the origin of in situ fluorescence is a collection of phytoplankton cells that are not spread by molecular diffusion and therefore it is not clear whether fluorescence can be considered a classic passive tracer or how the fluorescence field reacts to a turbulent flow field at microscales.

The goal is to establish the structure of the fluorescence field at high spatial wavenumbers. To that end, a high-resolution optical sensor was developed (Wolk et al. 2001) that is capable of resolving submeter scales of fluorescence. This sensor is routinely deployed with a vertical microstructure turbulence profiler (Wolk et al. 2002). To establish the fluorescence spectrum in high wavenumbers, the sensor's true three-dimensional spatial response must be known. To estimate the wave-

Corresponding author address: Fabian Wolk, Rockland Oceanographic Services Inc., 1112 Reno St., Victoria, BC V9A 4B6, Canada.
E-mail: Fabian@rocklandocean.com

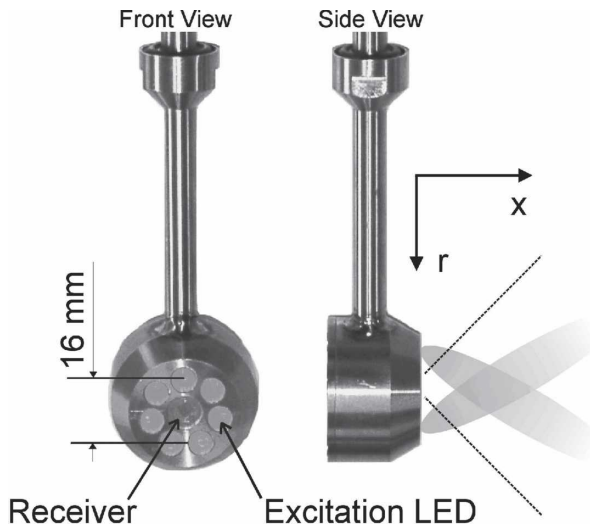


FIG. 1. (left) The front view of the sensor shows the excitation LEDs and the center receiver LED. (right) The side view shows the approximate beam pattern for two of the excitation LEDs. The dashed lines indicate the receiver diode's field of view. During deployment, the sensor travels in the r direction.

number response function of the sensor, it was mounted next to a fast-response thermistor and both sensors were towed through a warm, fluorescent plume. The thermistor is a point measurement of the turbulent field and the thermistor's response is unity in the lower-wavenumber band; the measured temperature signal can therefore be used as a proxy to describe the actual concentration variations in the turbulent field. The ratio of the measured power spectra of temperature and fluorescence then determines the transfer function of the fluorescence sensor. The test results show that the transfer function is a first-order, single-pole low-pass filter (Butterworth filter) with a half-power point at 22 cycles per meter (cpm).

2. Methods

a. Operating principle of the sensor

The high-resolution optical sensor is an open-path fluorometer. A set of light-emitting diodes (LEDs, Nichia NLPB310) produces the blue light required for fluorescence excitation (400–480 nm). The LEDs are arranged in a circle and are tilted 30° toward the center of this circle so that their light beams intersect (Fig. 1). The intersection of the light beams creates a sampling volume in front of the receiver diode. The reemitted light from the fluorescent material passing through the sampling volume is collected by the receiver diode, which is located at the center of the diode circle and which has an optical pass band of 640–720 nm. The

fluorometer is deployed on free-falling profiling instruments (Wolk et al. 2002) where it is mounted on the leading edge of the instrument so that the sampling volume is in the undisturbed flow region. Typical profiling speeds are $0.5\text{--}1\text{ m s}^{-1}$. The sensor travels in the r direction (Fig. 1), which minimizes the distortion of the flow field due to flow blockage by the sensor housing.

The intensity (or power) of the individual light beams (i.e., the directivity of the light source) is a function of the angle relative to the beam axis. At an off-axis angle of 20° , the light intensity is reduced by 50%. For practical purposes we therefore assume that the beam spread is approximately 40° . The arrangement of the LEDs creates a nearly conical, blurred sampling volume in front of the optical receiver diode. This receiver diode has an opening view angle of 45° . The point of the highest light intensity is 14 mm in front of the receiver diode, where the centerlines of the excitation light beams intersect. Away from this point, the light intensity decreases. The rate of decrease with distance from the intersection varies strongly depending on the spatial direction; for example, the decrease is strongest in the radial direction (r).

The complex geometry of the light sources makes it difficult to analytically predict the shape and size of the sampling volume, both of which determine the amount of spatial averaging. In earlier laboratory experiments (Wolk et al. 2001), summarized here in section 2b, the authors attempted to map the shape of the sampling volume using a fluorescent point source. These tests only gave coarse estimates and did not offer insight into the true wavenumber response of the sensor. The new experiments reported here are aimed at directly establishing the wavenumber transfer function, which gives an unambiguous measure of the sensor's spatial response.

b. Preliminary tests

The initial laboratory study was designed to determine the sensors response to artificial and naturally occurring fluorescent sources, and the extent of the sampling volume created by the excitation light. These tests were described in detail by Wolk et al. (2001) and are summarized here, because the original article is not published in the primary literature.

The sensitivity, linearity, and dynamic range of the probe were investigated by recording the sensor's output voltage for various concentrations of sodium fluorescein, pure chlorophyll a solutions, and natural phytoplankton assemblages. The samples were then analyzed using a Turner laboratory fluorometer 10R following Strickland and Parsons (1972). The sensor

output was fully congruent with the laboratory analysis of the samples, which confirmed that the sensor is capable of detecting single- and multispecies phytoplankton assemblages.

The general shape and size of the sampling volume was determined by recording the sensor output resulting from (i) a fluorescent point source, where the source was held at various distances along the x direction at $r = 0$; and (ii) strips of paper dyed with a fluorescent ink, where the strips were moved in the radial direction (r) in front of the sensor. The former experiment was carried out in a small aquarium filled with clear tap water, and it showed that the sensor output is well described by the relationship $V(x) = \lambda \exp(-x/10)$, where V is the sensor output voltage, x is the distance from the sensor (in mm), and $\lambda = 0.2$ V is an empirical scaling factor. The normalized cumulative integral of the modeled response $V(x)$ reaches 0.95 at a distance of $x = 33$ mm and 0.99 at a distance of $x = 49$ mm (see Wolk et al. 2001, their Fig. 6). The cumulative integral describes the fractional contribution of the source signal to the total contribution at a given distance x . The turbidity of the water affects these results, because the light backscatter from suspended particles decreases the amount of light detected by the sensor. The tests were conducted in clear water and, thus, represent a “worst case” scenario. In other words, the measured length of the sampling volume is an upper bound.

The approximate width of the sampling volume was established in the “strip experiment.” Fluorescent plastic strips, 10 mm wide, were mounted on a black cardboard surface, which was moved in a plane parallel to the sensor face in the r direction. This was done for several distances of the cardboard in front of the sensor. Fluorescent strips that were separated by more than 20 mm caused the sensor to register two distinct output pulses corresponding to the two strips passing in front of the sensor. Strips separated by less than 20 mm caused only one single pulse, regardless of distance between the sensor and the cardboard surface. Thus, the sensor performs a moving average in the r direction over a window with a maximum total width of 20 mm. This value is consistent with the diameter of the ring of excitation LEDs. The exact shape of the moving average window (e.g., box car, cosine, etc.) cannot be determined from this test. The strip test was initially carried out in air, as reported by Wolk et al. (2001); the same experiment was later carried out in water with identical results. Given by the cumulative integral of the sensor response in the x direction and the detectable separation in the r direction, we imagine the sampling volume to be an approximately ovaliform shape of length 49 mm and maximum width 20 mm.

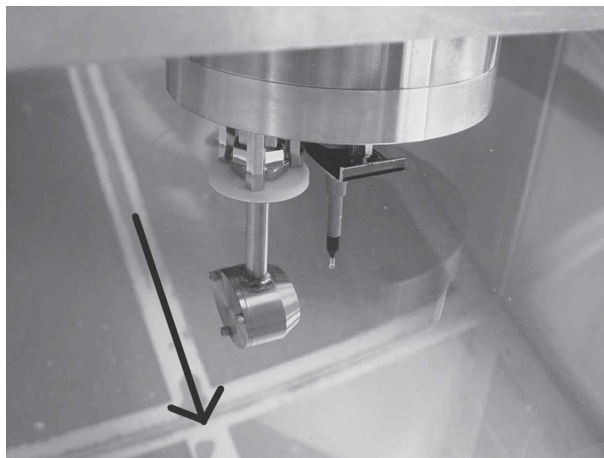


FIG. 2. Experimental setup for the transfer function measurement. (left) The fluorescence sensor and (right) the fast response thermistor are mounted underneath a carriage. The sensors are submerged ~ 0.1 m below the water surface. The carriage moves through the tank at a constant speed in the direction indicated by the arrow.

Based on the approximate width of the sampling volume (20 mm) and the typical profiling speed of $0.5\text{--}1$ m s^{-1} , the exposure time of the biological material during the free-fall operation is 20–40 ms. The fluorescence of various chlorophyll species reaches its peak in approximately 20 ms after illumination (Chekalyuk et al. 2000), and so the response of the sensor to the chlorophyll field can be assumed to be instantaneous.

c. Experimental setup

To determine the composite spatial response of the sensor, the fluorometer signal was compared to that of a fast-response thermistor (Thermometrics FP07). Both sensors were mounted on a carriage and towed in a tank through a warm, fluorescent plume (Fig. 2). The distance between the two sensors was 20 mm, while the sensing tip of the FP07 was within 5 mm of the center of the focal point of the light beams of the fluorescence sensor. As the carriage moved at a constant speed of 0.1 m s^{-1} , the fluorescent plume was created by pouring a stock solution of sodium fluorescein (concentration ~ 600 ppb) into the tank just in front of the moving carriage. The stock solution was heated to $\sim 5^\circ\text{C}$ above the water temperature in the tank.

Twelve runs of the experiment were carried out in the 10-m-long tank. For each run, data were recorded for a ~ 1.5 m section when the carriage speed was constant at $U = 0.1$ m s^{-1} . The sensor output voltages were sampled 256 times per second, digitized, and logged to a computer. The resulting time series of the output voltages were divided into 2048-point segments and the fast

Fourier transforms (FFTs) of the individual segments were averaged into one spectrum for temperature and fluorescence for each run (Oppenheim et al. 1999). Frequencies were converted to cyclic wavenumber using $k = U^{-1}f$. The length N of the FFT windows and the sampling rate of $F_s = 256$ Hz then gave a wavenumber resolution of $\Delta k = U^{-1}\Delta f = U^{-1}F_s/N = 1.25$ cpm and a resolved wavenumber range between 0 and 1280 cpm.

3. Results and discussion

a. Spatial transfer function

Any measured signal is related to the real physical quantity by the transfer function of the measurement system. To obtain the transfer function of the fluorescence sensor, it is assumed that

- (i) temperature variations can be used as a proxy tracer for variations fluorescein concentration and
- (ii) the transfer function of the temperature measurement system is unity.

If these assumptions hold, then the spatial transfer function $H^2(k)$ of the sensor can be estimated from the ratio of the fluorescence and temperature spectra:

$$H^2(k) = \Phi_{FF}(k)/\Phi_{TT}(k), \quad (1)$$

where $\Phi_{FF}(k)$ and $\Phi_{TT}(k)$ are the autospectra of fluorescence and temperature, respectively, and k is the cyclic wavenumber given by $k = f/U$.

The molecular diffusivity of the dye (sodium fluorescein, a salt) is approximately 100 times smaller than the diffusivity of the temperature. Based on the traveling speed of the carriage, the time between the injection of the warm dye into the water in front of the sensors and the detection of the injected dye by the sensors is ~ 1 s, so the differential diffusion of temperature and dye does not affect the detection of the fluorescence variations. In other words, the dye “stays” with the temperature signature.

At the carriage speed of $U = 0.1$ m s⁻¹ the FP07 thermistor has a time constant of $\tau = 0.01$ s, and we correct the measured temperature spectra with the sensor’s empirical response function (Gregg 1999):

$$H_{FP07}^2(f) = \frac{1}{[1 + (2\pi\tau f)^2]^2}. \quad (2)$$

The temperature spectrum shown in Fig. 3c is boosted by dividing the spectrum by the response function (2). At 10 Hz the correction applied to the measured spectrum is approximately a factor of 2. With this correction, the measured temperature signal can be regarded as a true representation of the turbulent field,

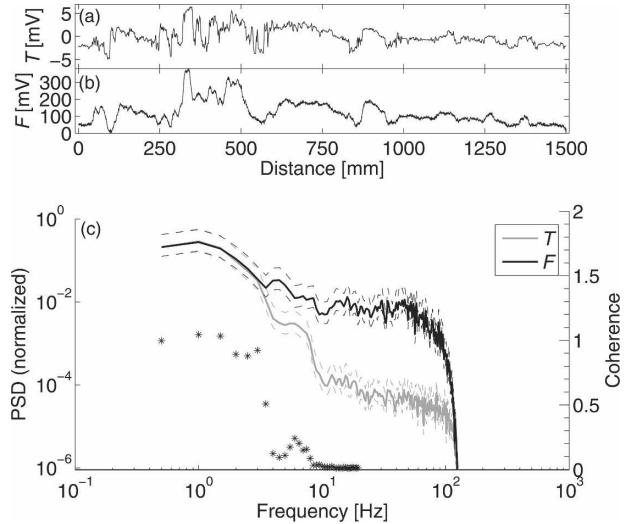


FIG. 3. Time series of (a) temperature and (b) fluorescence, and (c) the power spectral density of fluorescence and temperature of run 4 of the tank experiment. The time series are shown as output by the data recorder, in units of mV. The spectra are normalized by their respective total power. The temperature spectrum is corrected for the frequency response of the FP07 sensor. The frequency-dependent coherency between the F and T signals is shown as asterisks.

and the transfer function of the fluorometer can be estimated from (1).

Spectra are computed from the recorded time series of temperature, T , and fluorescence, F , as described in the previous section. A typical example of the time series and spectra of F and T is shown in Fig. 3. The data are from experimental run 4. Figures 3a and 3b show the signals of T and F , respectively, plotted against the distance traveled in the tank. The fluorescence signal clearly traces the slowly varying part of the temperature signal, but small-scale details of the temperature signal are not reflected in the fluorescence signal. The power spectra (Fig. 3c) corroborate this observation; they are congruent at frequencies up to 3 Hz and deviate at higher frequencies. Between 3 and 10 Hz, the temperature spectrum has four times more signal variance than the fluorescence spectrum. Both spectra flatten above 10 Hz, indicating the noise floor of their sensor-electronics systems. At ~ 80 Hz, the anti-aliasing filters of the recording systems sharply reduced the signal variances. The dashed lines indicate the approximate 95% confidence intervals for the spectra constructed from M segments of length 2048 points (Jenkins and Watts 1968).

The coherence spectrum, defined by

$$C_{FT}(k) = \frac{|\Phi_{FT}(k)|^2}{\Phi_{FF}(k)\Phi_{TT}(k)}, \quad (3)$$

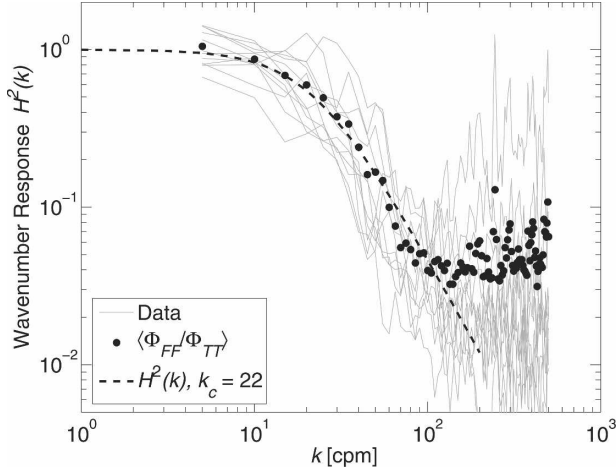


FIG. 4. Average wavenumber response (filled circle, ●) and model (dashed line). The gray lines are the transfer functions from individual runs. Frequency is converted to wavenumber using $k = f/U$. The spectra are truncated at 400 cpm.

where $\Phi_{FT}(k)$ is the cross spectrum, shows that the signals are coherent up to 3 Hz (or $k = 30$ cpm), which is equivalent to a length scale $L = k^{-1} = 0.033$ m. This length scale is consistent with the separation of the temperature and the fluorescence sensors (20 mm).

Figure 4 shows the results of the transfer function calculations. Gray lines are the transfer functions for the 12 separate runs, while solid circles show the ensemble averages of the individual transfer functions. The average transfer function is well approximated by the filter model:

$$H^2(k) = \frac{1}{1 + (k/k_c)^{2N}}, \quad (4)$$

with a half-power point at $k_c = 22$ cpm and $N = 1$. The parameters k_c and N were determined by minimizing the sum of the squared difference between the average transfer function and the model (4). This model is a first-order low-pass filter (or Butterworth filter), which we regard as the spatial transfer function of the sensor.

Since the transfer function estimated by (1) is based on the ratio of the output and input spectra of the measurement system (i.e., the sensor and its electronics), incoherent noise in the system introduces an asymptotic bias in the spectral ratio (1). This bias is evident in the measured transfer function above 100 cpm (Fig. 4), that is, where the dotted curve of the average transfer function flattens. Below 100 cpm (or 10 Hz) both $\Phi_{FF}(k)$ and $\Phi_{TT}(k)$ are clearly above the noise (Fig. 3c) and so the asymptotic noise bias does not affect our transfer function estimate. The fitted transfer function model (4) indicates a half-power point at 22 cpm, which is well

below the wavenumber band affected by the bias. At 22 cpm the power of $H^2(k)$ is a factor of 10 above the noise.

b. Averaging length scale

The 3-dB point of the transfer function (4) at $k_c = 22$ cpm determines a characteristic length scale over which the sensor will average in space. Intuitively, this “averaging scale” can be understood as the spatial scale below which the sensor will not be able to detect fluorescence variations. The fitted transfer function (4) describes a first-order system, for which

$$H^2(k) = \frac{1}{1 + (k/k_c)^2} = \frac{1}{1 + (\hat{k}/2\pi k_c)^2}, \quad (5)$$

where $\hat{k} = 2\pi k$ is the radian wavenumber. Introducing $l_c = (2\pi k_c)^{-1}$, we obtain

$$H^2(k) = \frac{1}{1 + (\hat{k}l_c)^2} = \frac{1}{1 + (2\pi k l_c)^2}, \quad (6)$$

which forms a Fourier transform pair with the spatial impulse response

$$h(x) = \frac{1}{l_c} \exp(-x/l_c). \quad (7)$$

In this representation, l_c is identified as a “response distance,” analogous to a time constant τ for the Fourier transform pair for time domain systems:

$$H^2(f) = \frac{1}{1 + (2\pi f\tau)^2} \quad \text{and} \quad h(t) = \frac{1}{\tau} \exp(t/\tau). \quad (8)$$

By this definition, the response distance, or averaging scale, is

$$l_c = \frac{1}{2\pi k_c} = 0.0072 \text{ [m]}. \quad (9)$$

It should be noted that the exponential averaging model (7) has no definite spatial limit; the weighting falls off exponentially and the scale l_c simply quantifies the filter behavior. If the sensor were moving into a sharp fluorescence interface, it would react to the step change with a response of 63% after penetrating $l_c = 0.0072$ m into the interface, 87% at $2l_c = 0.014$ m, and 95% at $3l_c = 0.022$ m. The value of l_c is consistent with the measured signals. Close inspection of the fluorescence signal (Fig. 3b) shows discernable signal changes on scales as small as 5–10 mm, for example, at distances of 50 mm, 320 mm, and others.

c. Spectra signal correction

The closed analytical form of the transfer function model (4) can now be easily used to correct measured

fluorescence spectra for the effects of the sensor's spatial averaging. The response-corrected spectrum Φ_{corr} is obtained by dividing the measured spectrum by the transfer function model; that is,

$$\Phi_{\text{corr}}(k) = \Phi_{\text{FF}}(k)[1 + (k/22)^2]. \quad (10)$$

Because of the noise considerations discussed above, we recommend that such a correction should only be applied up to a maximum wavenumber. This maximum wavenumber depends on the concentration of the fluorescence in the sample. A high concentration improves the signal-to-noise ratio and pushes the point where the spectrum reaches the noise floor to higher wavenumbers. In practice, therefore, any spectral correction cannot be carried out indiscriminately. Instead, a preliminary evaluation of the data available from a profile should be carried out to determine the maximum wavenumber to be used for individual sections of the profile with varying fluorescence concentrations.

4. Conclusions

An experimental method was presented that can be used to establish the spatial response of in situ fluorometers. The method works by comparing the spectral wavenumber response of the fluorometer to that of a reference sensor (here, a thermistor), which yields the spatial transfer function of the fluorometer. The described experimental setup and the data analysis can be adapted and applied to other optical sensors.

The initial evaluation of the fluorometer described here shows that the sensor's sample volume can be roughly imagined as an ovaloid with a diameter of approximately 20 mm and a length of 49 mm. The spatial averaging, however, is not uniform but weighted in the optical focal point, leading to effective smaller-scale resolution. Application of the described method shows that the measured composite spatial transfer function fits the model of a first-order low-pass filter with a 3-dB wavenumber at $k_c = 22$ cpm. Based on the 3-dB wave-

number, the characteristic averaging scale of the sensor is 7 mm. Fluorescence variations on that length scale will be detected by the sensor at 63% of the true signal level.

Acknowledgments. The authors thank Jim Mitchell and Laurent Seuront for their helpful advice and critical e-mail discussions, which helped in the preparation of this manuscript. This work was partially supported by Grant-in-Aid for Science Research (B2) 16310005 from the Japan Society for the Promotion of Science.

REFERENCES

- Batchelor, G. K., 1967: *An Introduction to Fluid Mechanics*. Cambridge University Press, 635 pp.
- Chekalyuk, A., F. Hoge, C. W. Wright, and R. N. Swift, 2000: Short-pulse pump-and-probe technique for airborne laser assessment of Photosystem II photochemical characteristics. *Photosyn. Res.*, **66**, 33–44.
- Corsin, S., 1951: On the spectrum of isotropic temperature fluctuations in isotropic turbulence. *J. Appl. Phys.*, **22**, 469–473.
- Derenbach, J. B., H. Astheimer, H. P. Hansen, and H. Leach, 1979: Vertical microscale distribution of phytoplankton in relation to the thermocline. *Mar. Ecol. Prog. Ser.*, **1**, 187–193.
- Gregg, M. C., 1999: Uncertainties and limitations in measuring ϵ and χ_T . *J. Atmos. Oceanic Technol.*, **16**, 1483–1490.
- Jenkins, G. M., and D. G. Watts, 1968: *Spectra Analysis and Its Applications*. Holden-Day, 525 pp.
- Mann, K. H., and J. R. N. Lazier, 1996: *Dynamics of Marine Ecosystems: Biological–Physical Interaction in the Ocean*. 2d ed. Blackwell Science, 350 pp.
- Oppenheim, A. V., R. W. Schaffer, and J. R. Buck, 1999: *Discrete-Time Signal Processing*. 2d ed. Prentice-Hall, 870 pp.
- Seuront, L., and P. G. Strutton, Eds., 2004: *Handbook of Scaling Methods in Aquatic Ecology*. CRC Press, 600 pp.
- Strickland, J. D. H., and T. R. Parsons, 1972: A practical handbook of sea-water analysis. *J. Fish. Res. Bd. Can.*, **167**, 311 pp.
- Wolk, F., L. Seuront, and H. Yamazaki, 2001: Spatial resolution of a new micro-optical probe for chlorophyll and turbidity. *J. Tokyo Univ. Fish.*, **87**, 13–21. [Available from Tokyo University of Marine Science and Technology, 4-5-7 Konan, Minato-Ku, Tokyo 108-8477, Japan.]
- , H. Yamazaki, L. Seuront, and R. G. Lueck, 2002: A new free-fall profiler for measuring biophysical microstructure. *J. Atmos. Oceanic Technol.*, **19**, 780–793.